applied sciences

MDPI

Article

Analysis of Load-Sharing and Contact Characteristics of the Concentric Face Gear Split-Torque Transmission System with Elastic Supports

Fei Gong [1], Rupeng Zhu [1,*], Pingjun Li [2] and Guanghu Jin [1]

[1] National Key Laboratory of Science and Technology on Helicopter Transmission, Nanjing University of Aeronautics and Astronautics, Nanjing 210016, China; gongfei1189@163.com (F.G.); meeghjin@nuaa.edu.cn (G.J.)
[2] AECC Hunan Aviation Powerplant Research Institute, Zhuzhou 412002, China; research1986@163.com
* Correspondence: rpzhu_nuaa@163.com

Abstract: The concentric face gear split-torque transmission system (CFGSTTS) is a new form of drive that is primarily used in helicopter transmission systems. Its load-sharing performance among different branches and tooth contact characteristics have a great impact on the service life of helicopter transmissions. It contains ten meshing pairs, the load distribution is complicated, and the tooth contact areas are difficult to determine. Therefore, based on the multi-point constraint method and nonconforming grid, a quasi-static analysis model of the CFGSTTS coupled with flexible supports was established and the load-sharing performance and contact characteristics were studied. The model considered the support stiffness, backlash, installation error, and web structure of the upper face gear, which could comprehensively reflect the meshing state of the system. The load-sharing coefficient curves, tooth contact area diagram, and meshing force were obtained. The results indicated that (1) a larger idler support stiffness and a smaller input gear support stiffness could achieve better load equalization performance; (2) better load equalization between idler gears could be acquired with a lower face gear support stiffness factor of approximately 0.9; (3) increasing the axial mounting error caused the contact area to shift to the top and inner end of the face gear tooth, which was detrimental to the transmission; and (4) adjusting the backlash of the idler gears, input gears, and tail gear had little influence on the load balance and contact.

Keywords: concentric face gear; split torque; multi-point constraint; load sharing; contact area

Citation: Gong, F.; Zhu, R.; Li, P.; Jin, G. Analysis of Load-Sharing and Contact Characteristics of the Concentric Face Gear Split-Torque Transmission System with Elastic Supports. *Appl. Sci.* **2022**, *12*, 4894. https://doi.org/10.3390/app12104894

Received: 26 March 2022
Accepted: 10 May 2022
Published: 12 May 2022

1. Introduction

As early as the middle of the last century, research on face gears began [1,2], which provided the foundation for face gear applications. Nevertheless, it has long been the case that face gears are mainly used in light load applications. It was not until the 1990s that the application of face gears in aerospace transmission mechanisms caused face gears to become a progressively hot research topic. Litvin [3] conducted a detailed study on the tooth surface geometry and tooth contact analysis of face gears. Subsequently, McDonnell Douglas combined a face gear split-torque drive system with a conventional planetary gear system to reduce the mass of a new helicopter transmission system by 40%, demonstrating a significant mass advantage of a face gear split-torque drive [4]. Furthermore, a sequence of tests [5–7] demonstrated that face gears can operate at high speeds and under heavy loads. Filler [8] tested a face gear split-torque transmission system and showed that face gears can be effectively applied to rotorcraft gearboxes with weight-saving and cost-reduction benefits.

The split-torque gear drive can realize multi-channel shunting of power and has the advantages of compact structure, small size, and being lightweight, but it also faces the problems of load sharing and fatigue life. According to the collected literature, the fatigue problem of split-torque gear transmission has been less studied. Ding [9] developed a fatigue life assessment method for spur gears based on the Lundberg–Palmgren fatigue life theory and Hertz contact theory for helicopter split-torque transmission systems. As for the marine split-torque herringbone gear transmission system, Zhao [10] carried out a study on the correlation between vibration energy and fatigue life and obtained the variation law of fatigue life with vibration energy. On the other hand, the load-sharing problem of split-flow transmission systems has always been the focus of research. Face gears are mainly used in helicopter main reducers in the form of split-flow transmission. In the coaxial face gear split-torque transmission system, the difference in meshing stiffness caused by the difference in the upper and lower face gear structure and the existence of manufacturing error and assembly error leads to the load borne by each branch gear to be different between gears. Consequently, the research on the load-sharing characteristics has a certain reference significance for the load-sharing design of the system.

The studies concerning the load sharing of split-torque drives are mainly confined to planetary gear transmission and cylindrical gear split-torque and combined power transmission. Using the contact mechanics model of planetary gears, Bodas [11] conducted a study on the influence of manufacturing and assembly errors of planetary carriers and gears on the load distribution amongst planets under quasi-static conditions and quantified the load-sharing behavior. Lu et al. [12] modeled a 2K-H type planetary transmission system from the perspective of dynamics, calculated the floating amount of the basic components under load-splitting and equalization requirements, and analyzed the dynamic load-sharing characteristics and the effect of error variation; the analysis results showed that the floating sun wheel could improve the load sharing of the system. Gui et al. [13] constructed a bending–torsion coupling dynamic model of a double-input cylindrical gear split transmission system and calculated the system load-sharing coefficient using a numerical method. The results showed that the torsional stiffness of the double gear shaft had a great influence on the load sharing. Sun et al. [14] established a dynamic model of a two-stage helical planetary gear transmission system considering gear backlash and errors, studied the load-sharing performance of four load-sharing structures, and proposed a method for calculating the dynamic sensitivity of the load distribution coefficient to errors. Mo et al. [15] studied the load distribution between star gears in a two-stage star gear transmission system, built a mathematical model for calculating the load-sharing coefficient considering the displacement coordination, and obtained the curve of the load-sharing coefficient. Then, Mo et al. [16] analyzed the load distribution mechanism of the star gear reducer, established a calculation model of the load-sharing coefficient accounting for the comprehensive meshing errors, and obtained the curves of the influences of the errors on the load-sharing coefficient. Du et al. [17] established a load distribution analysis model for a two-stage star gear transmission and systematically investigated its load distribution behavior. Dong et al. [18] established a static-load-sharing calculation model of a two-stage five-branch planetary gear train and introduced the loading tooth contact analysis method to analyze the effects of manufacturing errors, installation errors, and the floating amount on the load-sharing coefficient. Wang et al. [19] developed a dynamic model of a multi-stage planetary gear transmission system of a wind turbine by employing the lumped parameter method and explored the load-sharing behavior under the action of time-varying input speed and internal excitation.

In addition to the studies on the load sharing of planetary gears, according to the collected literature, a few scholars have also studied load sharing for systems containing face gears in earlier times. In 2002, Heath [20] set up a complex load-sharing test platform for a face gear split-torque drive and the test results showed that the load-sharing coefficient between the two face gears at the input gear was 1.083 and the load-sharing coefficient between the two idle gears was 1.33, which verified the feasibility of using a face gear in the torque-sharing systems. Chun [21] studied the load distribution and sharing of a face gear split-torque transmission system using both the classic method and the finite element method. Zhao et al. [22] established the analysis model of a helicopter face gear split-torque transmission system and the results showed that the load-sharing performance can be improved using floating supports.

Coaxial face gear split-torque transmission systems have become a hot research topic recently. Zhao et al. [23,24] analyzed the uneven load mechanism for the concentric face gear split-torque transmission and investigated the influence of system parameters on the load-sharing performance. Dong et al. [25] combined the finite element method (FEM) and the analytical method (AM) to investigate the effects of the distribution angle of pinions and the load conditions on the meshing stiffness of the gear pairs in the CFGSTTS. Subsequently, Dong et al. [26,27] determined the power direction of the CFGSTTS using the finite element method; investigated the effect of system parameters on the power direction; and discussed the influences of torsional stiffness, backlash, and time-varying meshing stiffness on the dynamic load distribution through the lumped parameter model. Li et al. [28] analyzed the main factors that affect the load distribution of the concentric face gear split-torque transmission, established a bending–torsion–shaft coupling centralized parametric dynamic model, and investigated the influence of support stiffness and no-load transmission errors on the dynamic-load-sharing performance. Mo et al. [29,30] developed a translation–torsion dynamic model of a coaxial face gear split-torque transmission system, obtained the meshing force curve and load distribution coefficient curve, and then analyzed the effects of various factors on the load distribution coefficient.

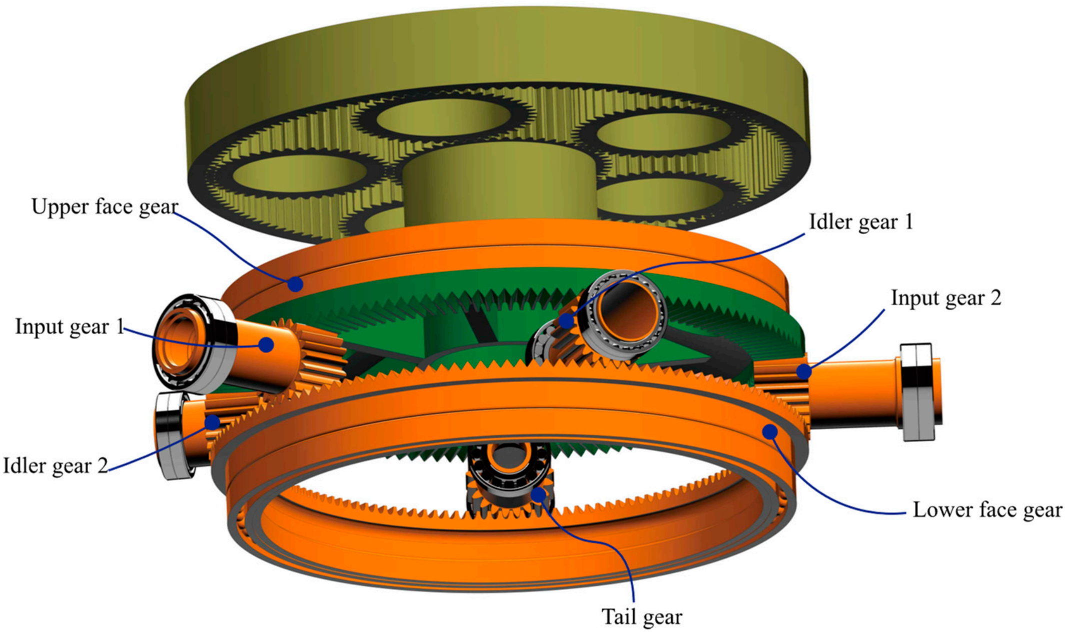

Figure 1. Schematic diagram of the concentric face gear split-torque transmission system.

Due to manufacturing and assembly errors, as well as the structural differences between the upper and the lower face gears, the loads on each branch gear of the concentric face gear split-torque transmission system vary. Moreover, for the practical engineering application of a face gear power-split transmission configuration, the theoretical calculation of the tooth surface contact force and the tooth surface contact area under a load condition is complicated because there are many gear pairs in contact at the same time and there are few reports in the literature. Therefore, based on the existing research, we carried out an analysis of the load sharing, meshing force, and tooth surface contact area by constructing a quasi-static analysis model of the concentric face gear split-torque transmission system with coupling elastic support. The schematic diagram of the research object is illustrated in Figure 1. It consisted of two face gears and five pinions, and the face gears were coaxially placed face-to-face. First, according to the principle of gear meshing and the method of rotating projection, the mapping model of tooth surface meshing was established, and the nonlinear equations containing tooth surface parameters were formed. The parametric segmentation method was used to provide initial values for the Newton–Raphson algorithm, and the digital tooth surface was calculated to provide tooth surface data for parametric modeling. Then, the spring element was used to simulate the support stiffness, and the coupled elastic support system model was established based on the multi-point constraint method. Lastly, the influence of the elastic support stiffness parameters, face gear installation errors, and backlashes on the load sharing and contact characteristics were evaluated using the single factor analysis method.

2. Numerical Model of the Face Gear Surface

The tooth surface of the face gear was generated using an involute spur shaper cutter through a certain movement; the coordinate system is shown in Figure 2. The coordinate systems S_{S0} and S_{20} were fixed to describe the initial positions of the spur gear cutter S and the machined face gear. The coordinate systems S_S and S_2 rotated with the spur gear cutter S and the machined face gear, respectively. The coordinate origin of S_S, S_2, S_{S0}, and S_{20} was located at the intersection of the axis of cutting tool S and the rotation axis of the machined face gear.

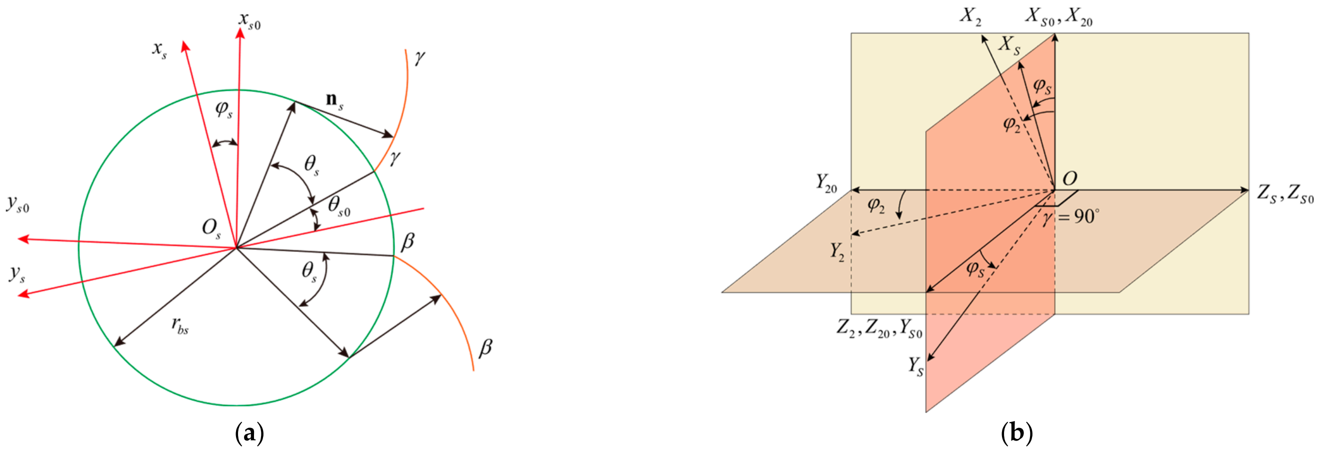

Figure 2. Diagrams showing the processing of the face gear: (**a**) parameters of the involute surface of the gear cutter and (**b**) generating coordinate system of face gear.

The tooth surface Σ_s of the spur gear cutter was established according to the involute equation as follows:

$$r_s(u_s, \theta_s) = \begin{cases} \pm r_{bs}(\sin(\theta_{os} + \theta_s) - \theta_s \cos(\theta_{os} + \theta_s)) \\ -r_{bs}(\cos(\theta_{os} + \theta_s) + \theta_s \sin(\theta_{os} + \theta_s)) \\ u_s \end{cases} \tag{1}$$

where u_s and θ_s are the tooth surface parameters of the cutter gear; r_{bs} is the radius of the base circle; '$\pm$' represents the involutes $\gamma - \gamma$ and $\beta - \beta$, respectively; and θ_{os} is expressed as:

$$\theta_{os} = \frac{\pi}{2N_s} - \tan(\alpha_0) + \alpha_0 \tag{2}$$

where N_s is the number of teeth of the gear cutter and α_0 is the pressure angle.

The unit normal vector n_s of a point P on Σ_s is expressed as follows:

$$n_s = \frac{\frac{\partial r_s}{\partial \theta_s} \times \frac{\partial r_s}{\partial u_s}}{\left| \frac{\partial r_s}{\partial \theta_s} \times \frac{\partial r_s}{\partial u_s} \right|} \tag{3}$$

The cutter gear was used as a generating gear, and the face gear tooth surface Σ_2, which was conjugated to the cutter tooth surface, was developed in accordance with the relative motion relationship between the two tooth surfaces. Based on the meshing principle, the tooth surface Σ_2 could be obtained according to the following equation:

$$\begin{cases} r_2(u_s,\theta_s,\varphi_s) = M_{2,20}M_{20,S0}M_{S0,S}r_s(u_s,\theta_s) \\ n_s \cdot v_s^{S2} = f(u_s,\theta_s,\varphi_s) = 0 \end{cases} \tag{4}$$

where $M_{2,20}$, $M_{20,S0}$, and $M_{S0,S}$ are the coordinate conversion matrices, v_s^{S2} is the relative motion speed of the cutting tool and the tooth surface of face gear at the meshing point, and the position vector r_2 indicates the tooth surface equation of Σ_2.

The transition surface Σ_2^* of the face gear was formed using the tooth top of the cutting tool. This meant that the top line of the cutting tool was transformed into the surface Σ_2^* formed in the fixed coordinate system of the face gear using a homogeneous coordinate transformation. The angle parameter θ_s in the tooth profile equation of the cutting tool was replaced by the parameter at the addendum circle θ_s^*, and the equation of the tooth top could be derived.

Similar to the principle of generating the tooth surface, the transition surface equation $r_2^*(u_s,\varphi_s)$ expressed in the coordinate system S_2 was as follows:

$$r_2^*(u_s,\varphi_s) = M_{2,20}M_{20,S0}M_{S0,S}r_s^*(u_s,\theta_s^*) \tag{5}$$

If undercutting did not occur, there was a common tangent L between the tooth fillet surface Σ_2^* and the working surface Σ_2 and its equation was as follows:

$$\begin{cases} r_L(u_s^*,\varphi_s) = M_{2,20}M_{20,S0}M_{S0,S}r_s(\theta_s^*,u_s) \\ f(u_s^*,\theta_s^*,\varphi_s) = 0 \end{cases} \tag{6}$$

The tooth surface of the face gear is a complex spatial surface. In this study, the coordinates of discrete tooth surface points of the face gear were obtained using the rotating projection mapping method. First, the minimum inner radius R_1 and the maximum outer radius R_2 of the face gear were obtained by solving the conditions to avoid undercutting and tooth tip sharpening. The tooth top position r_{sm} and the tooth root position r_{as} were obtained through the parameters of the cutting tool, and then the range of the tooth surface of the face gear on the projection plane was determined, as shown in Figure 3. O_L is the intersection of the cutting tool axis with the face gear axis. Finally, the grid planning of the projection plane was carried out, the mapping relationship between the grid points and the tooth surface coordinates was established and the grid parameters were obtained by solving the nonlinear equations.

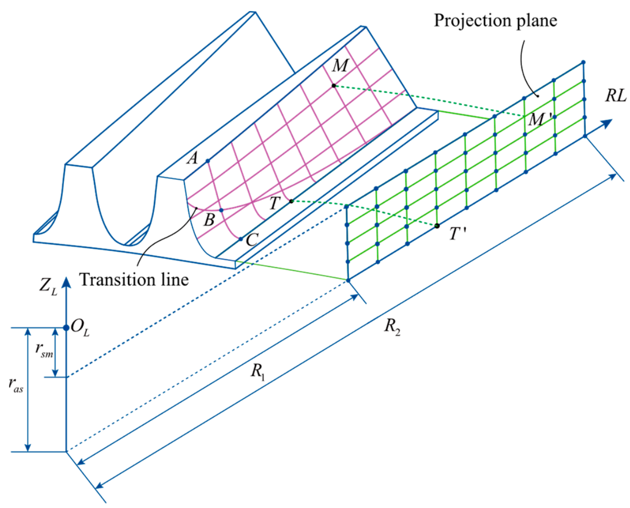

Figure 3. The mapping between the tooth surface and the rotating projection plane.

In Figure 3, the point M on the working surface of the face gear is three-dimensional, and its coordinates are ($x_M(\theta_s, \varphi_s)$, $y_M(\theta_s, \varphi_s)$, $z_M(\theta_s, \varphi_s)$). The corresponding point of M in the rotating projection plane is M', and its coordinates are (RL, ZL). The equation could be obtained from the rotational projection relation:

$$\begin{cases} z_M(\theta_s, \varphi_s) = ZL \\ x_M^2(\theta_s, \varphi_s) + y_M^2(\theta_s, \varphi_s) = RL^2 \end{cases} \quad (7)$$

Similarly, the point T on the fillet surface of the face gear was three-dimensional, and its coordinates are ($x_T(u_s, \varphi_s)$, $y_T(u_s, \varphi_s)$, $z_T(u_s, \varphi_s)$). The corresponding point of T in the rotating projection plane is T', and its coordinates are (RL, ZL). The equation can be obtained from the rotational projection relation as follows:

$$\begin{cases} z_T(u_s, \varphi_s) = ZL \\ x_T^2(u_s, \varphi_s) + y_T^2(u_s, \varphi_s) = RL^2 \end{cases} \quad (8)$$

Equations (7) and (8) are nonlinear equations, which need to be provided with initial values near the zero point when solved using Newton's method. However, Newton's method is sensitive to the initial value, and if the initial value is not appropriate, a solution that does not match the expectation may be obtained. In this study, a parametric partitioning method was used to provide the initial values [31]. As shown in Figure 3, ABC is the tooth profile of the face gear at a certain radius, where AB is the working tooth profile, BC is the transition tooth profile, and point B is on the transition line. The equation parameters of the working tooth surface are (θ_s, φ_s) and those of the transition tooth surface are (φ_s, u_s). θ_{As} and θ_{Bs} denote the values of parameter θ_s when the cutting tool meshes with the face gear at points A and B, respectively. φ_{Bs} and φ_{Cs} denote the values of parameters φ_s when the tool and face gear are engaged at points B and C, respectively. The initial parameter values of the equations of AB and BC were calculated separately, and the steps were as follows.

(a) On the working tooth profile, the parameters θ_{As}, θ_{Bs}, and φ_{As} were obtained according to Equations (9) and (10). Divide θ_{As} to θ_{Bs} equally into θ_{ns} subsections, substitute them into Equation (11) as known parameters, and then solve Equation (11) to obtain φ_{ns}. Take (θ_{ns}, φ_{ns}) as the initial value for solving Equation (7).

(b) On the transition surface, φ_{Bs} and φ_{Cs} were obtained using Equations (11) and (12), and then φ_{Bs} and φ_{Cs} were equally divided into φ_{ks}, which were substituted into Equation (13) to solve for u_{ks}. (φ_{ks}, u_{ks}) was then taken as the initial value for solving Equation (8).

$$\begin{cases} x_M^2(\theta_{As}, \varphi_{As}) + y_M^2(\theta_{As}, \varphi_{As}) = RL^2 \\ z_M(\theta_{As}, \varphi_{As}) = r_{sm} \end{cases} \quad (9)$$

$$\theta_{Bs} = \frac{\sqrt{r_{as}^2 + r_{bs}^2}}{r_{bs}} \quad (10)$$

$$x_M^2(\theta_{ns}, \varphi_{ns}) + y_M^2(\theta_{ns}, \varphi_{ns}) = RL^2 \quad (11)$$

$$\varphi_{Cs} = \arctan\theta_s^* - \theta_{s0} - \theta_s^* \quad (12)$$

$$x_M^2(\theta_s^*, \varphi_{ks}, u_{ks}) + y_M^2(\theta_s^*, \varphi_{ks}, u_{ks}) = RL^2 \quad (13)$$

3. Quasi-Static Analysis Model

The accurate calculation of the meshing force is the prerequisite for the study of the load-sharing characteristics of the concentric face gear split-torque transmission system. Generally, the smaller the mesh cell size is in the FEA, the more continuous the contact stress distribution on the tooth's surface and the more accurate the meshing force results, but it leads to a higher computational cost. For this issue, some methods were proposed to balance the computational accuracy and computational cost [22–33]. Accordingly, the coupled elastic support and mesh non-coordinated face gear model was established based on the multi-point constraint method, as shown in Figure 4.

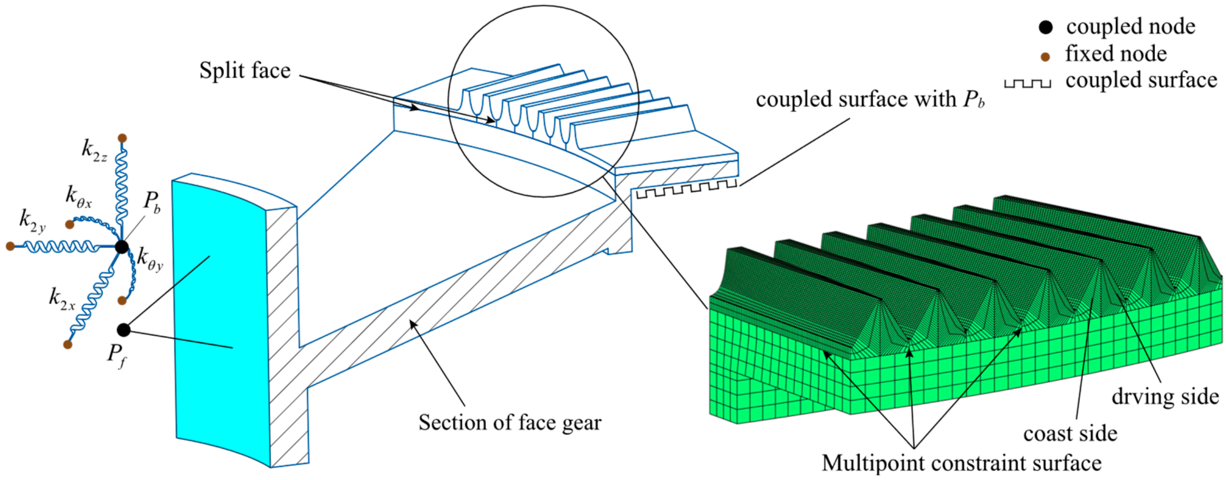

Figure 4. Schematic diagram of the finite element model of the upper face gear.

Figure 4 shows the FEA model of the upper face gear. The teeth of the upper face gear were separated from the hub, the teeth were discretized using fine meshes, and the rim was discretized using coarse meshes. The nonconforming mesh interface was connected using a multi-point constraint algorithm. In addition, the driving and coast sides of the face gear were meshed with grids of different sizes, and the coupling connection was carried out at the tooth root segmentation based on the MPC method. Meanwhile, to reduce the number of computational nodes, just the teeth engaged in the meshing were retained.

In finite element analysis, solid elements generally have no rotational degrees of freedom. An additional node needs to be created when applying the boundary conditions of torque and angular displacement. The node P_f in Figure 4 was coupled with the internal surface of the face gear hub to apply the boundary conditions. The node P_b was coupled to the bottom surface of the upper face gear rim and was used as a moving node of the spring element. In Figure 4, k_{2x}, k_{2y}, k_{2z}, $k_{\theta x}$, and $k_{\theta y}$ are the x-radial, y-radial, z-axial, x-angular and y-angular stiffnesses of the spring element in the local coordinate system of the upper face gear, respectively. The red dot in the figure is considered to be a fixed node of the spring element.

Figure 5 shows the finite element model of the cylindrical gear coupled with elastic support. Six teeth were reserved at the meshing with the upper and lower face gears. P_{c1} was an auxiliary node connected to the inner surface of the cylindrical gear. First, it allowed the cylindrical gear to apply torque and angular displacement, and additionally, it acted as a moving node for the spring element. In the figure, P_{c2} and P_{c3} are the fixed nodes of the spring element. k_{ix} and k_{iy} are the radial stiffnesses of the cylindrical gear support. The schematic diagram of the transmission system model is shown in Figure 6.

In addition, applying the convergence criteria of force and displacement in the solution and reducing the convergence values were beneficial for the accuracy of the results. The basic geometric parameters of the concentric face gear split-torque transmission system are shown in Table 1 and the support stiffness values are listed in Table 2. The input torque of the single input gear was 1256 Nm and the output torque of the tail transmission was 251 Nm. The elastic modulus of the gear material was E = 206 GPa and the Poisson's ratio was $\mu = 0.3$. The coordinate system of the model was a Cartesian coordinate system. The x-axis and y-axis of the face gear were radial, and the z-axis coincided with the axis of the face gear pointing to the upper face gear. The x-axis and y-axis of the cylindrical gear were radial, the z-axis was axial, and the y-axis pointed to the lower face gear. The contact forces of each meshing pair were compared under elastic support and rigid support of the system in Figure 7, respectively. From the figure, it can be seen that when considering elastic support, the fluctuation range of the meshing force was small, and the numerical value of the contact force was quite different from that of the rigid support. Therefore, it was necessary to consider elastic support when analyzing the load-sharing characteristics of the system.

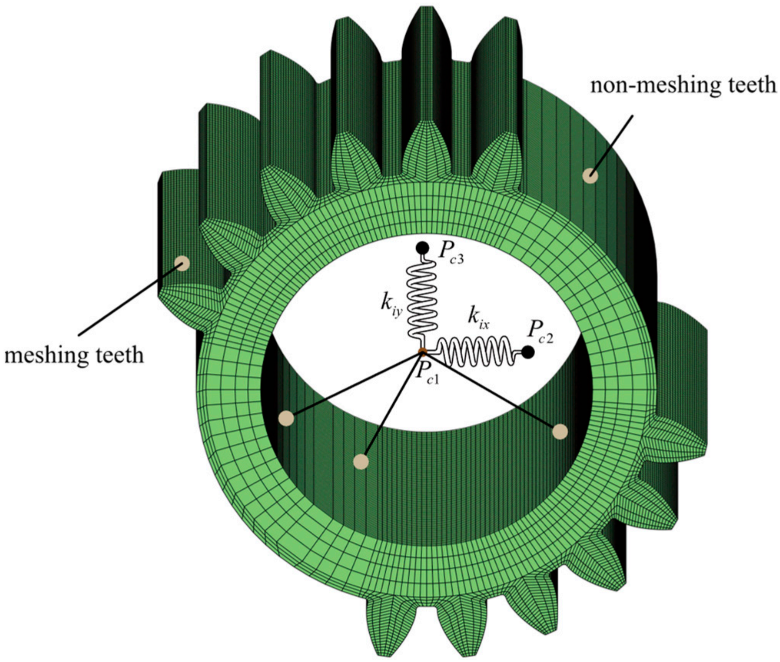

Figure 5. Schematic diagram of the pinion finite element model.

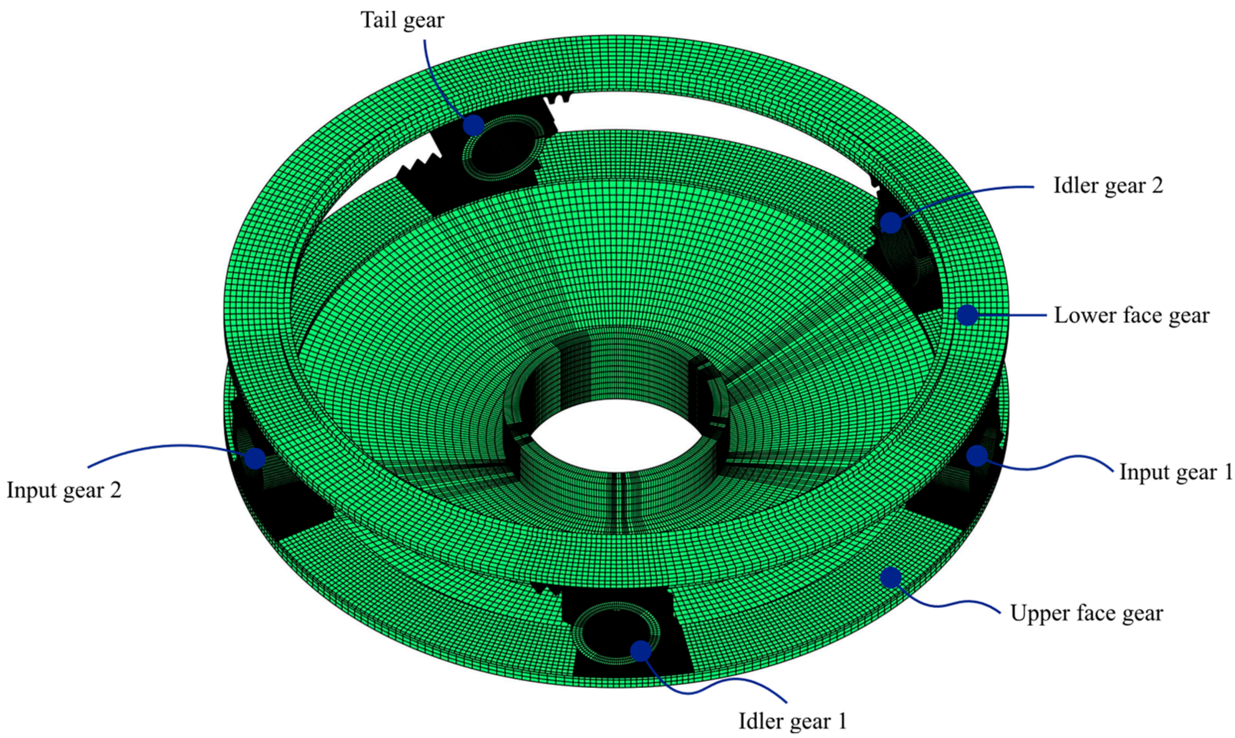

Figure 6. Schematic diagram of the finite element model of the transmission system.

Table 1. Main parameters of the concentric face gear split-torque transmission system.

Parameters	Value	Parameters	Value
Number of gear cutter teeth	22	Shaft angle	90°
Number of pinion teeth	21	Pressure angle	25°
Number of face gear teeth	142	Addendum height coefficient	1
Normal modulus	3.9 mm	Top clearance coefficient	0.25

Table 2. The values of gear support stiffness.

	k_x (N/mm)	k_y (N/mm)	k_z (N/mm)	$k_{\theta x}$ (Nmm/rad)	$k_{\theta y}$ (Nmm/rad)
Input gear	6.58×10^5	6.58×10^5	/	/	/
Idler gear	7.53×10^5	7.53×10^5	/	/	/
Upper face gear	2.60×10^6	2.60×10^6	1.44×10^6	4.78×10^{10}	4.78×10^{10}
Lower face gear	1.20×10^7	1.20×10^7	1.01×10^7	3.79×10^{11}	3.79×10^{11}
Tail gear	6.20×10^5	6.20×10^5	/	/	/

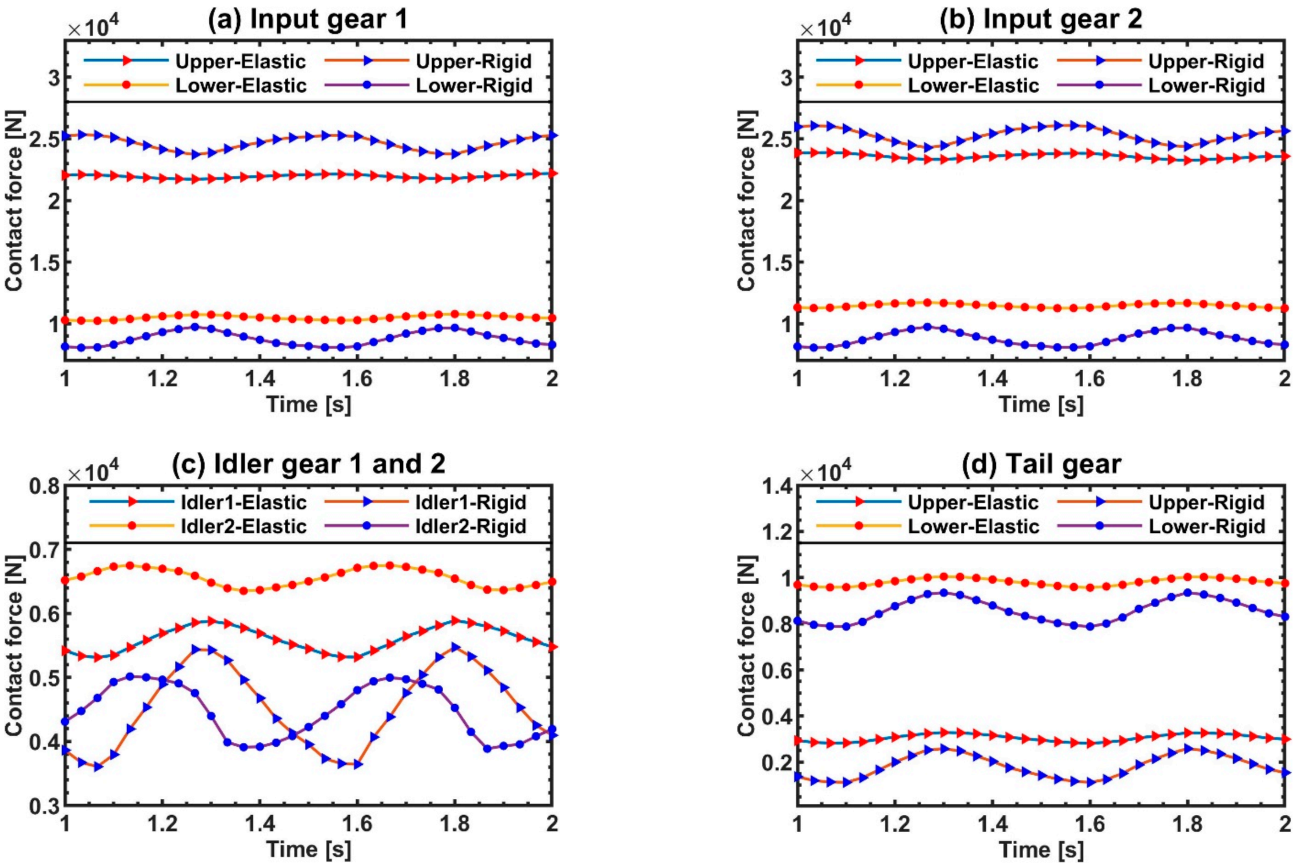

Figure 7. Comparison of the meshing force between the elastic support and rigid support.

4. Discussion

For convenience, idler gear 1, idler gear 2, input gear 1, input gear 2, and the tail gear are represented by the numbers 1, 2, 3, 4, and 5, respectively, and the upper and lower face gears are denoted by the numbers 6 and 7, respectively. Five pinions and two face gears formed ten meshing pairs, which were recorded as M_{ij} (I = 1~5, j = 6,7). Through the quasi-static finite element analysis model, the meshing force F_{ij} of each meshing pair shown in Figure 7 could be calculated. Then, the load-sharing coefficient between idler gear 1 and idler gear 2, i.e., ζ_{id}, was defined as follows:

$$\zeta_{id} = \frac{2\max(\text{mean}(F_{16}), \text{mean}(F_{26}))}{\text{mean}(F_{16}) + \text{mean}(F_{26})} \tag{14}$$

The load-sharing coefficient of the upper and lower face gears at input gear, i.e., ζ_{in}, was defined as follows:

$$\zeta_{in} = \frac{2\max(\text{mean}(F_{36}), \text{mean}(F_{37}))}{\text{mean}(F_{36}) + \text{mean}(F_{37})} \tag{15}$$

where max() and mean() are the maximum and mean functions, respectively.

A quasi-static analysis under dual-input and dual-output operating conditions was carried out to study the effect of the variation of support stiffness on the load sharing and tooth contact area, as well as the meshing force. The support stiffness of each gear was set to κk, where k is the original stiffness value and $\kappa \in [0.1, 10]$ is the stiffness adjustment factor. When analyzing the influence of the support stiffness of a single gear, the support stiffness of other parts remained unchanged. The load-sharing coefficient ζ, the tooth contact area, and the meshing force of each meshing pair were obtained using the finite element method. In addition, to verify the correctness of the model, the results of this paper were compared with the results of Figure 6 in similar reference [28].

4.1. Support Stiffness

Figure 8 shows the variation in the system's load-sharing coefficient, contact area, and meshing force with the support stiffness factor of the idler gear. F_m and F_p in Figure 8g are the mean values of the meshing force and the fluctuation amplitude, respectively. As shown in Figure 8a, the load-sharing coefficient of the idler gear slowly increased from 1.04 at 0.1 times the support stiffness to 1.13 at 10 times the support stiffness, and the load-sharing coefficient of the input gear rapidly decreased from 1.52 at 0.1 times the support stiffness to 1.23 at 10 times the support stiffness. Moreover, both load-sharing coefficients changed rapidly in the range of (0.1, 1). Furthermore, the influence trend of the support stiffness of the idler gear on the load-sharing coefficient of the input gear was consistent with Figure 6 in reference [28]. Figure 8b–f clearly indicate that the idler support stiffness had little effect on the contact area of the input–face gear pair. In contrast, it had an obvious influence on the contact area of the idler face gear pair and the tail face gear pair. As seen in Figure 8g, as the stiffness increased, the power transmitted from the input gear to the lower face gear increased, while the power transmitted to the upper face gear through the tail gear decreased, and the changed power of these two parts was transmitted to the upper face gear through the idler gear. Therefore, not only could the contact characteristics of the idler gear pair be adjusted by changing the support stiffness of the idler gear but the power transmitted by each gear pair could be adjusted to make the load more balanced.

The influences of the support stiffness of the input gear on the load-sharing coefficient, contact area, and meshing force are explored in Figure 9. It can be seen in Figure 9a that increasing the support stiffness of the input gear significantly increased the load-sharing coefficient of the idler gear and the input gear, where the load-sharing coefficient of the input gear rapidly increased from 1.07 to 1.60. Furthermore, both load-sharing coefficients varied quickly in the range of (0.1, 1). Similar to Figure 6 of [28], the input gear stiffness had a greater effect on the load-sharing performance of the input gear. As shown in Figure 9b–f, the input gear support stiffness had little effect on the contact area of the input–upper face gear pair. However, the contact area of other gear pairs clearly decreased when the stiffness increased. Figure 9g shows that as the stiffness decreased, the power transmitted by the input gear to the lower face gear increased and then transmitted to the upper face gear through the idler gear. In summary, a smaller input gear support stiffness was more conducive to the control of the load-sharing coefficient and contact area.

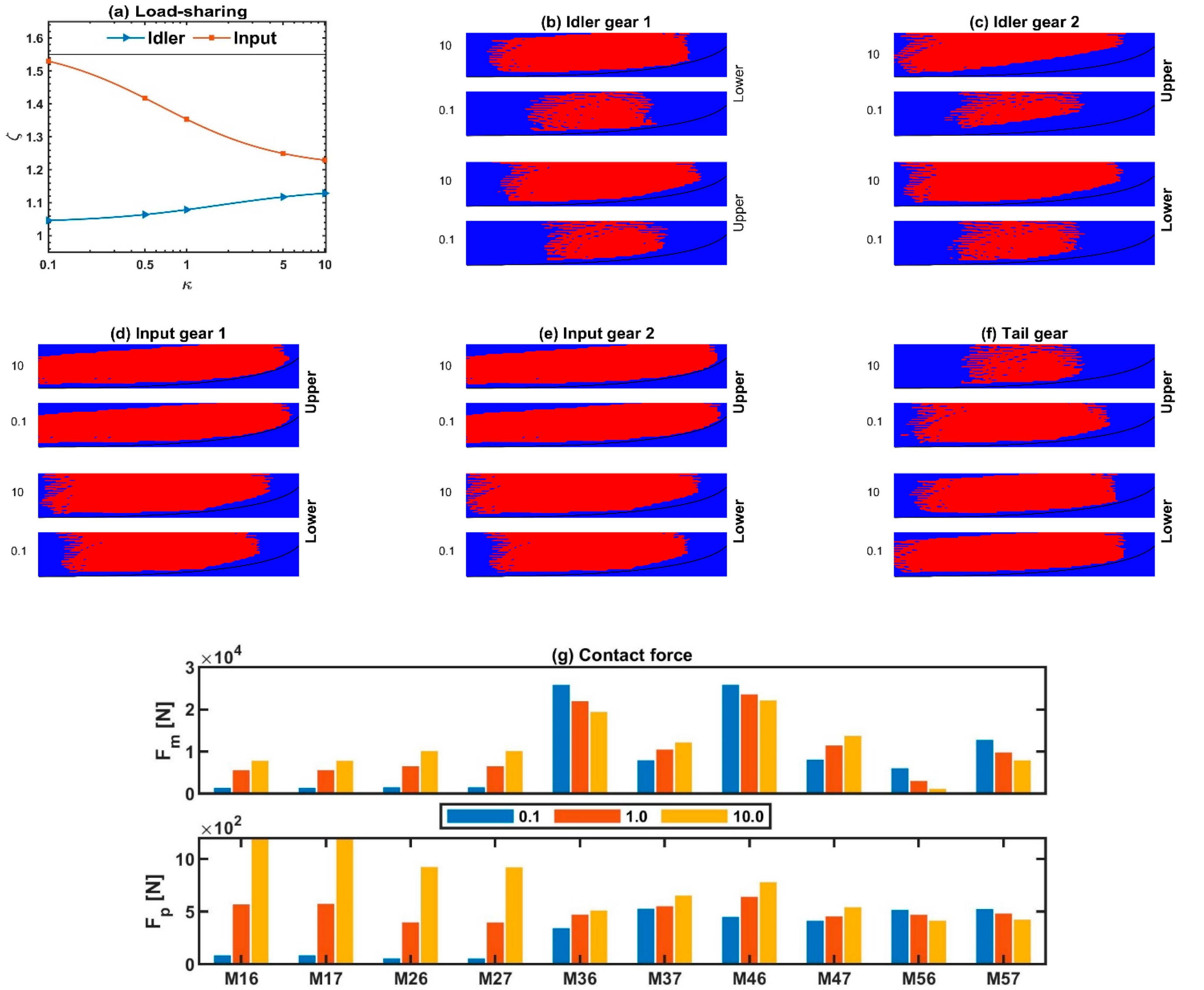

Figure 8. Influence of the support stiffness of the idler gear on the load-sharing and contact characteristics.

Figure 10 shows the influence of the support stiffness of the tail transmission gear on the load-sharing coefficient, contact area, and meshing force of each gear pair. As can be seen in Figure 10a, with an increase in the support stiffness of the tail transmission gear, the load-sharing coefficient of the input gear changed significantly compared to that of the idler gear, and the greater the stiffness coefficient, the gentler the change was. In Figure 6 of [28], the load-sharing coefficient of the input gear decreases with the increase of the tail gear support stiffness, which is consistent with the conclusion of this study. As can be seen in Figure 10b–g, with the increase in the stiffness factor, the contact area of the tail gear pair increased significantly such that the tail gear bore more load. This also reduced the maximum load transmitted in the idler gear and the input gear meshing pair. Therefore, the large tail support stiffness was more conducive to a balanced bearing.

Figure 11 shows the influence of the support stiffness of the upper gear on the load-sharing coefficient, the contact area, the mean value of the meshing force, and the fluctuation amplitude of the meshing force. Figure 11a shows that increasing the support stiffness of the upper face gear slightly increased the load-sharing coefficient of the input gear. However, the load-sharing coefficient of the idler gear reduced significantly, from 1.33 when the supporting stiffness was 0.1 to 1.004 when the supporting stiffness was 10 and decreased rapidly in the range of (0.1, 1). As can be seen in Figure 11b–f, with an increase in the support stiffness of the upper face gear, the contact area of the idler gear 1–upper face gear pair expanded and the contact spot was offset to the outer end. The related conclusion can be obtained from Figure 11g, where increasing the upper face gear support stiffness increased the mean value of the contact force of idler gear 1 and minimized the difference with the mean value of the contact force of idler gear 2. Hence, the load equalization factor of the idler gear was reduced. The large stiffness coefficient reduced the contact area of the meshing pairs M56 and M57, and the average meshing force slowly decreased. This meant that the power transmitted to the upper face gear through the tail gear became smaller, and more power was transmitted through idler gear 1. Consequently, the load-sharing coefficient and power transmission path could be controlled to a certain extent by adjusting the support stiffness of the upper face gear.

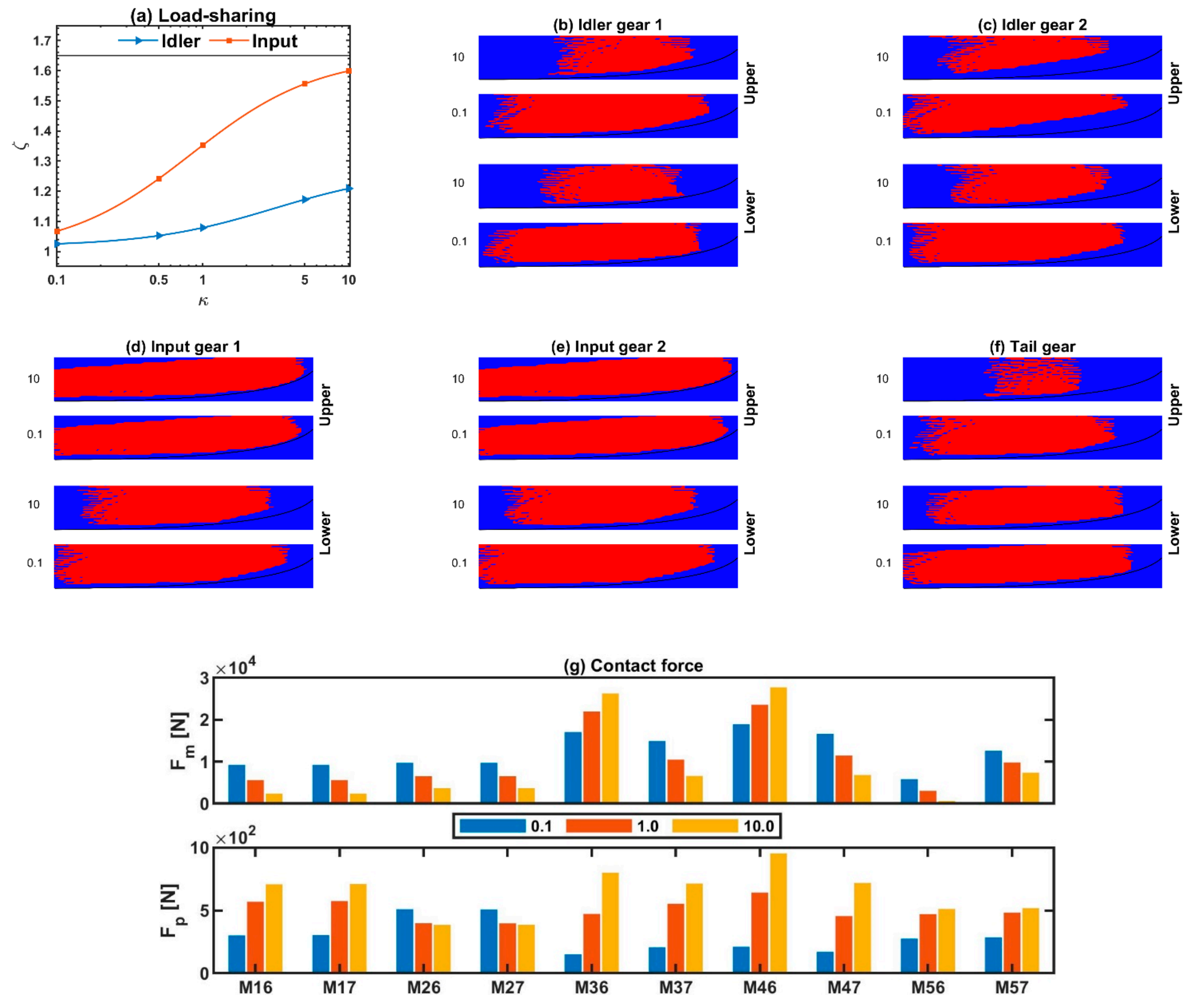

Figure 9. Influence of the support stiffness of the input gear on the load-sharing and contact characteristics.

As can be seen in Figure 12a, increasing the support stiffness of the lower face gear significantly reduced the load-sharing coefficient of the input gear. However, the load-sharing coefficient of the idler gear first decreased and then increased. When the stiffness coefficient was about 0.9, the load-sharing coefficient was the smallest. It can be seen in Figure 12b–f that changing the support stiffness of the lower face gear had the greatest impact on the contact characteristics of the idler gear–face gear pair. Similarly, increasing the lower face gear support stiffness significantly increased the average contact force of idler gear 2 and gradually exceeded that of idler gear 1. Therefore, the load-sharing coefficient decreased first and then increased. In general, increasing the support stiffness of the lower face gear increased the power transmitted from the input gear to the lower gear and output this power to the upper face gear through idler gear 2.

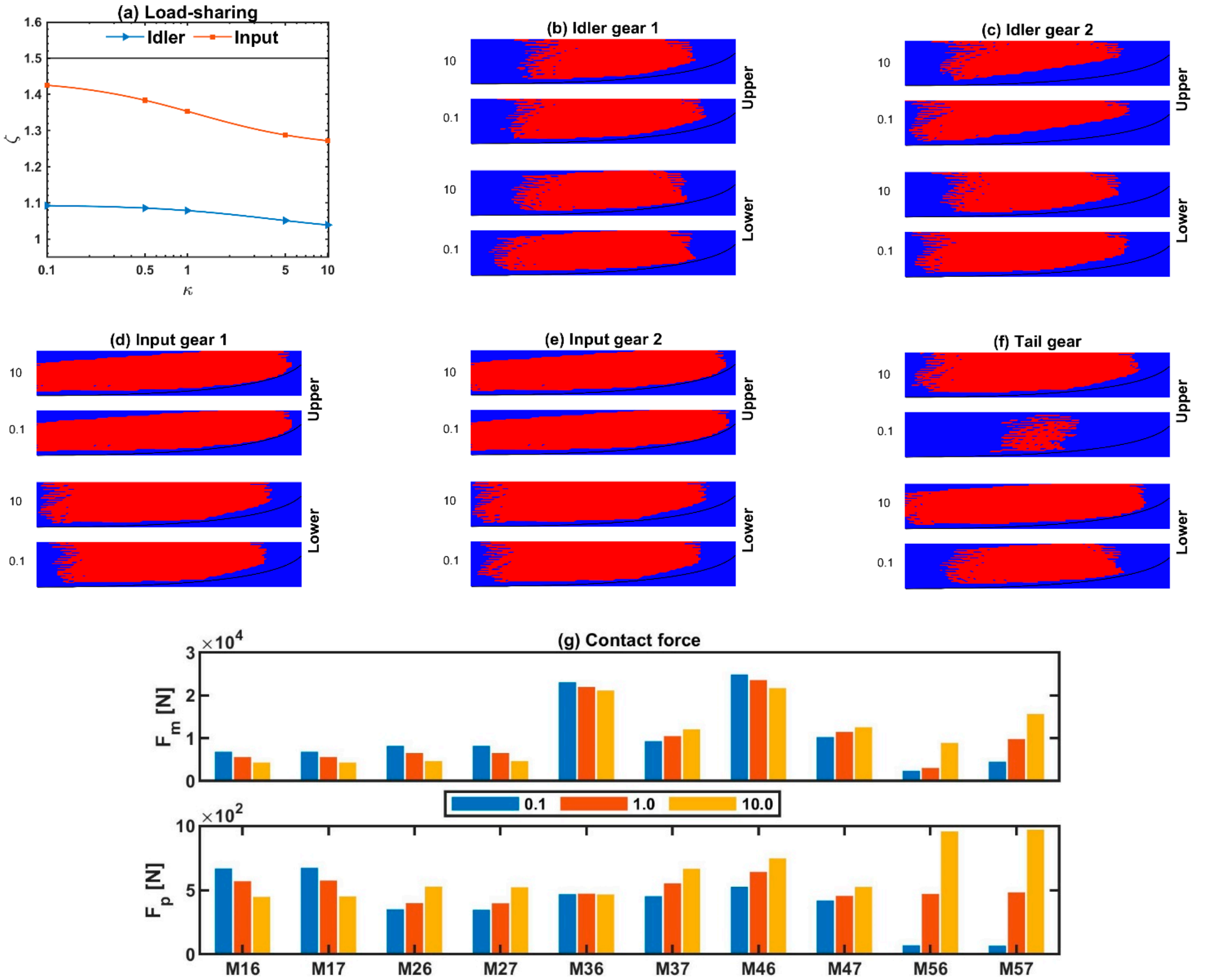

Figure 10. Influence of the support stiffness of the tail gear on the load-sharing and contact characteristics.

To further investigate the effects of the angular, axial, and radial components of the upper and lower face gear support stiffness on the load-sharing characteristics, the results obtained using quasi-static analysis are shown in Figures 13 and 14. In these figures, subfigures (a), (b), and (c) show the effects of the angular, axial, and radial stiffness on the load sharing, respectively. It can be seen that the angular stiffness of the upper face gear had a great impact on the load sharing of the idler gear. When the stiffness factor exceeded 1, the influence on load sharing gradually decreased.

4.2. Axial Mounting Error of the Face Gear

Generally, face gear drives adjust the backlash by adjusting the face gear axial mounting position. Therefore, to analyze the effect of the axial mounting error on the load-sharing and contact characteristics, the axial installation error was analyzed, as shown in Figure 15.

Δu and Δl indicate adjusting the upper and the lower face gears, respectively. The analysis results are shown in Figures 16 and 17.

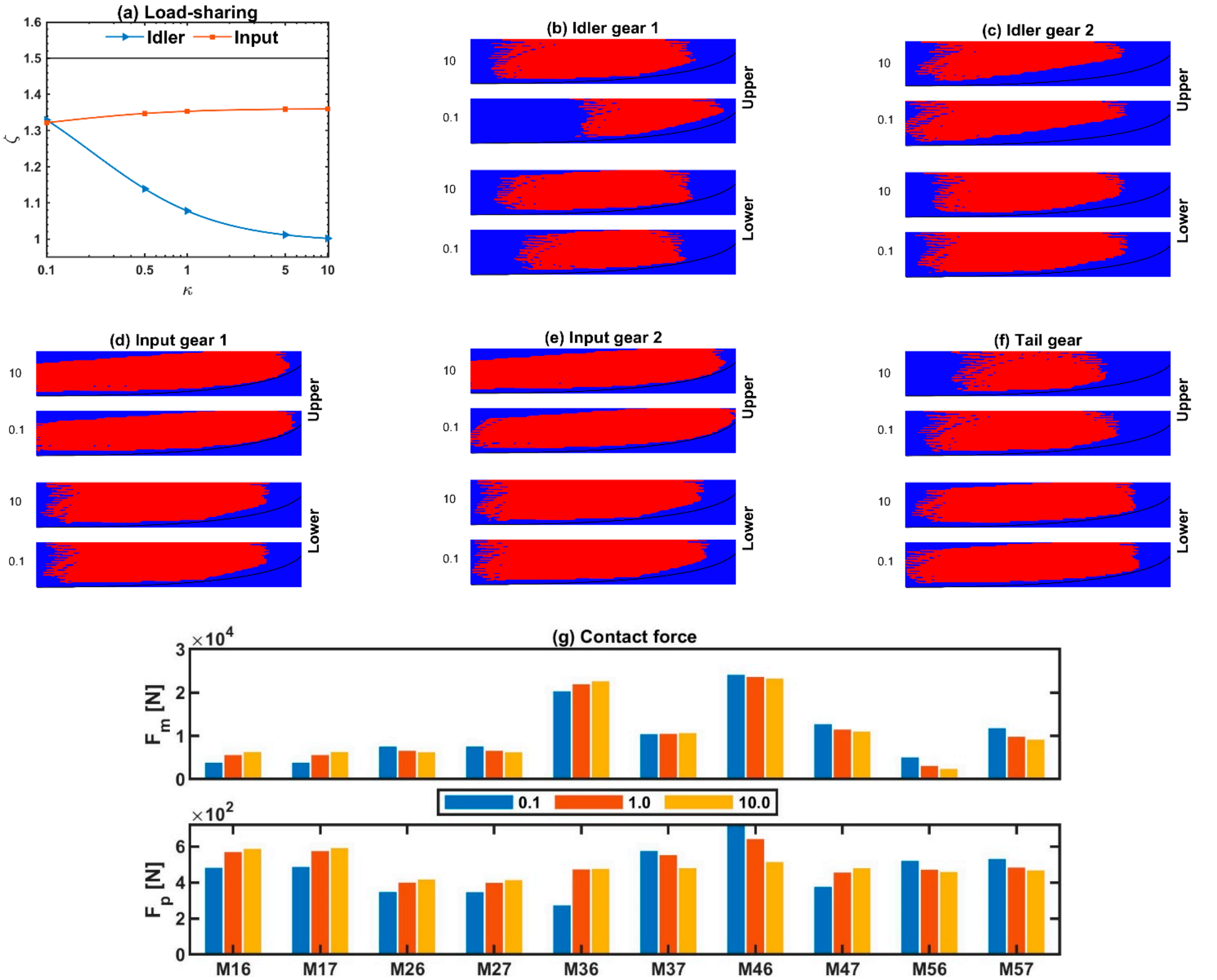

Figure 11. Influence of the support stiffness of the upper face gear on the load-sharing and contact characteristics.

It can be seen in Figure 16a that increasing the axial installation error of the upper face gear slightly reduced the load-sharing coefficient of the idler gear and the input gear. However, as can be seen in Figure 16b–f, the contact characteristics of the upper face gear deteriorated, and the contact area was not only reduced but also offset to the inner end. Furthermore, there was no significant change in the mean value of the contact force for each meshing pair, which meant that the contact stress on the upper face gear increased significantly. Likewise, the installation error of the lower face gear also had a great impact on the contact characteristics of the lower face gear. With the increase in the installation error of the lower face gear, the load-sharing coefficient of the idler gear and the input gear increased. This showed that if the backlash was adjusted by the axial installation of the face gear, its value range could be properly controlled.

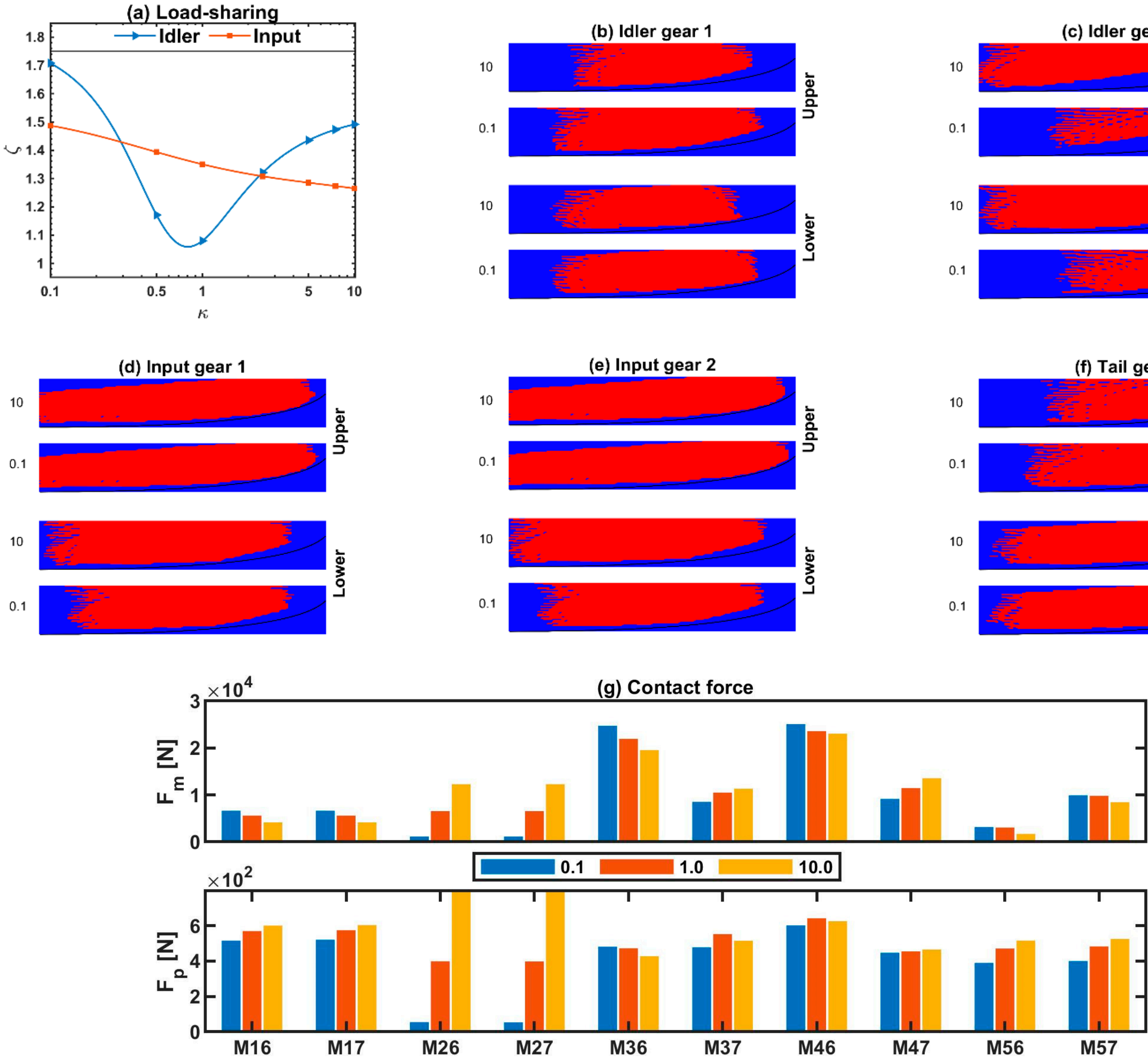

Figure 12. Influence of the support stiffness of the lower face gear on the load-sharing and contact characteristics.

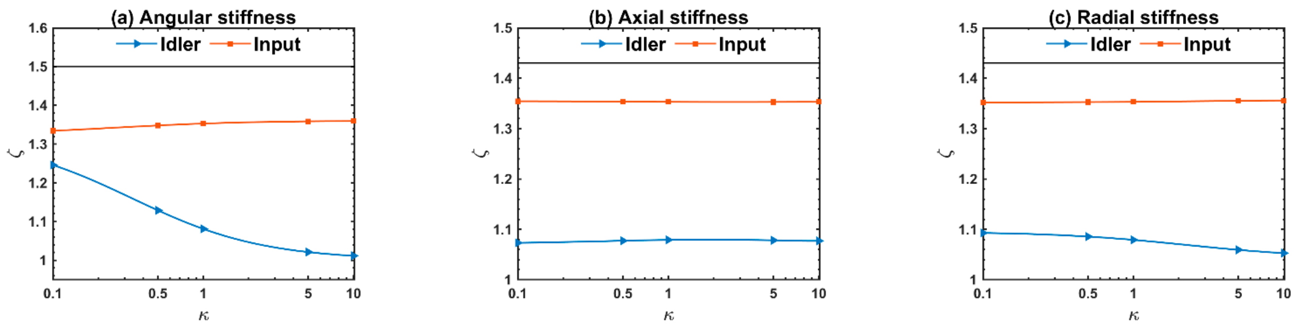

Figure 13. Influence of the angular, axial, and radial stiffness of the upper face gear on the load sharing .

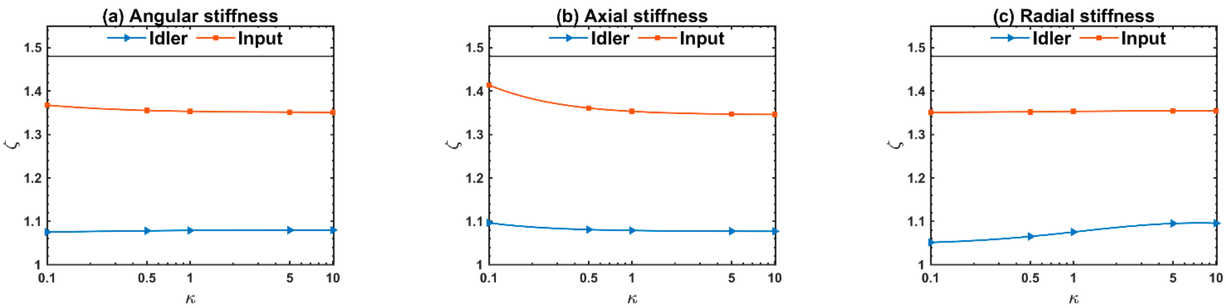

Figure 14. Influence of the angular, axial, and radial stiffness of the lower face gear on the load sharing.

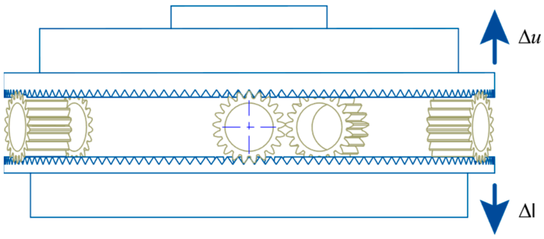

Figure 15. Diagram of the mounting error of a face gear.

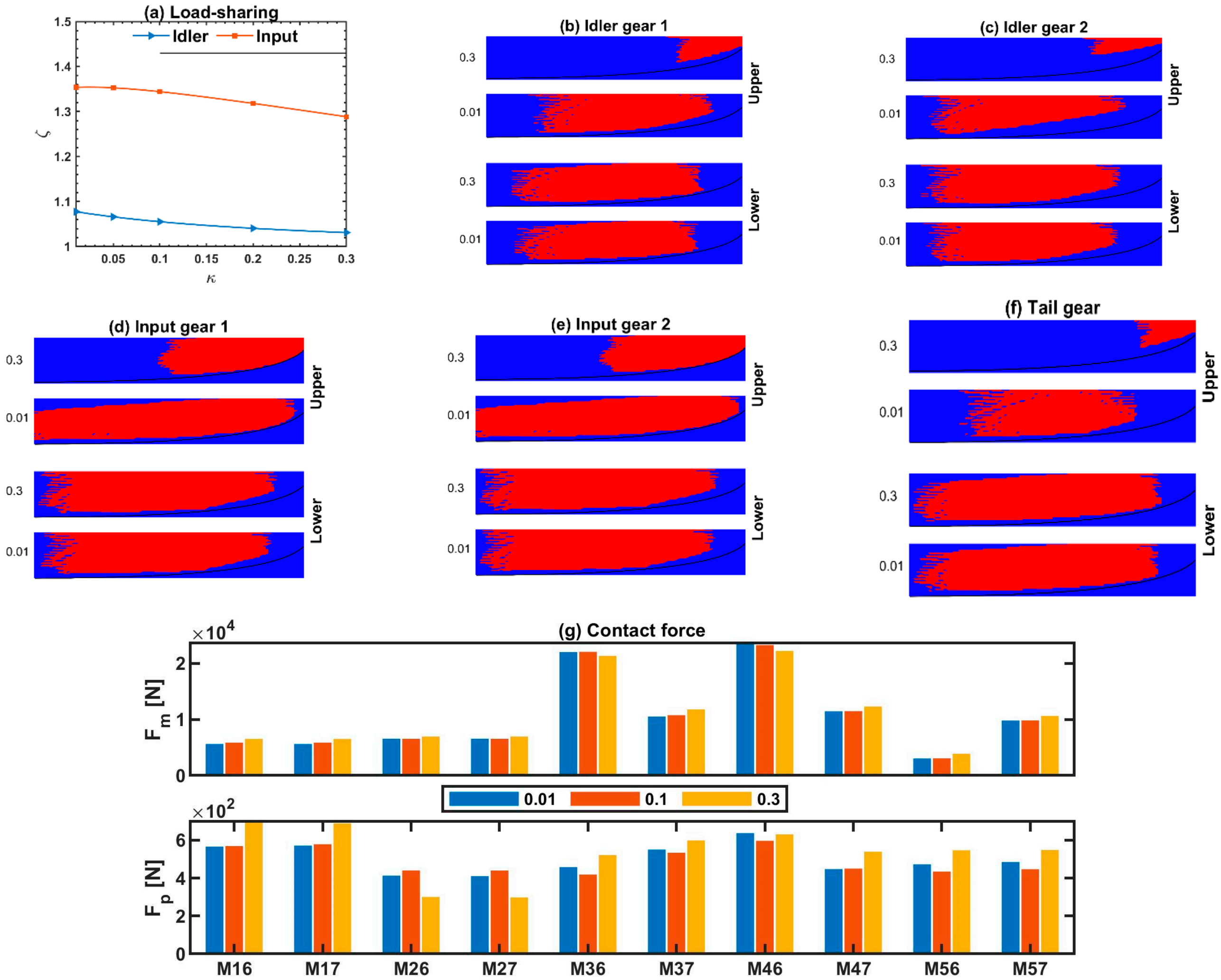

Figure 16. Influence of the axial installation error of the upper face gear on the load-sharing and contact characteristics.

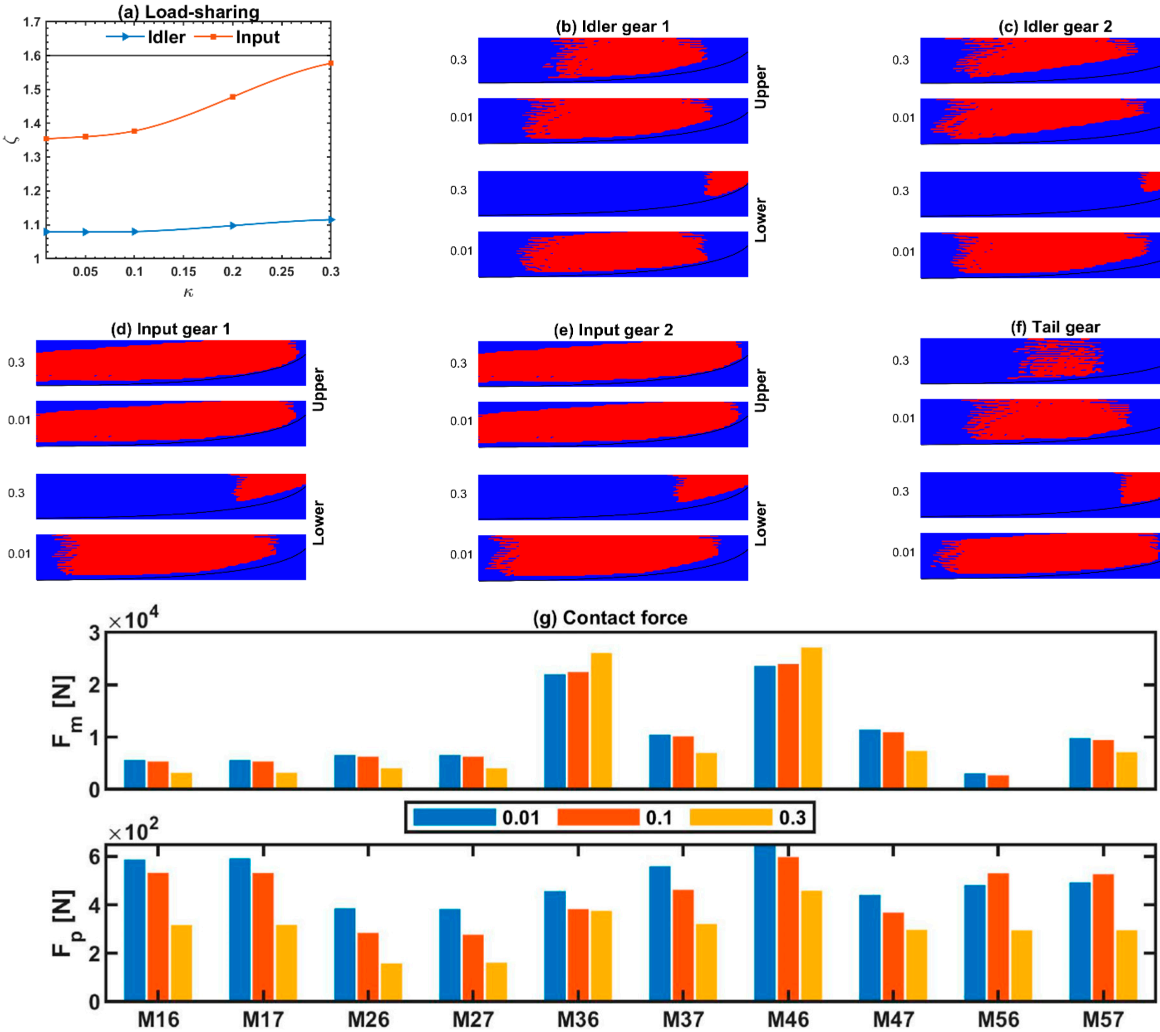

Figure 17. Influence of the axial installation error of the lower face gear on the load-sharing and contact characteristics.

4.3. Backlash

The backlash b_h, as shown in Figure 18, is an important parameter in gear dynamics analysis. In this study, by changing the backlash of each of the idler gear, input gear, and tail transmission gear, the influence of the backlash on the load sharing and contact characteristics was analyzed under the condition that the other parameters remained unchanged. Figure 19 shows that the backlash had little effect on the load-sharing coefficient. Taking the idler gear backlash as an example, when the backlash values were 10 μm and 100 μm, the load-sharing coefficients of the idler gear were 1.079 and 1.078, respectively, which decreased slightly.

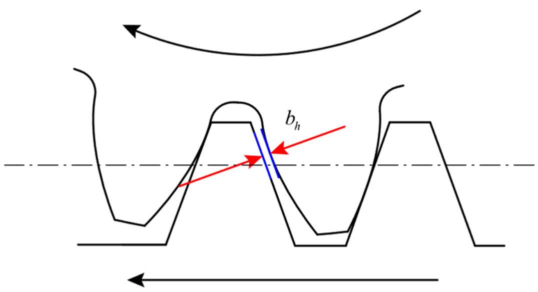

Figure 18. Schematic diagram of backlash.

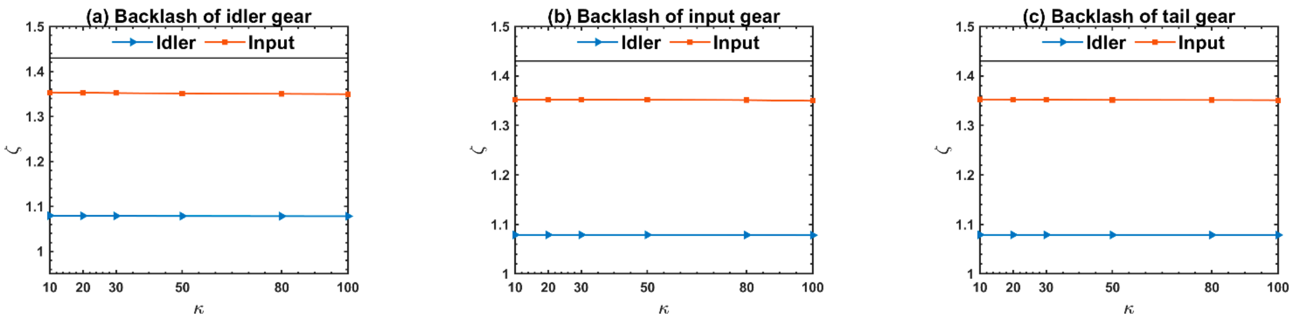

Figure 19. Influence of the backlash on the load-sharing coefficient.

5. Conclusions

In this study, considering the problem of multiple meshing pairs and complex load distribution of the concentric face gear split-torque transmission system, a quasi-static analysis model with coupled elastic support was constructed based on the multi-point constraint method. To balance the solver time and solution accuracy, the meshes of the driving side and coast side were controlled with different dimensions using the grid non-coordination principle. Then, the trend analysis of the load-sharing and contact characteristics was carried out using the single factor analysis method. The effects of the elastic support stiffness parameters, face gear installation error, and backlash on the load-sharing and contact characteristics were studied. By analyzing the calculation results, the conclusions were as follows:

1. The support stiffness had less influence on the contact characteristics of the input face gear pair. Therefore, in the adjustment of the contact performance of the concentric face gear drive, the other gear pairs could be adjusted under the premise of ensuring proper contact characteristics of the input face gear pair.
2. Adjusting the pinion support stiffness could modify the load-bearing of each gear pair to make it more balanced; a larger support stiffness of the idler gear and tail gear and a smaller support stiffness of the input gear could reduce the load-sharing coefficient.
3. Increasing the support stiffness of the upper face gear was beneficial for lowering the load-sharing coefficient of the idler gear, and the load-sharing coefficient of the input gear did not change significantly, whereas it would be more appropriate when the factor of the support stiffness of the lower face gear was approximately 1.0.
4. The increase in the axial installation error of the upper and lower face gears obviously deteriorated the contact characteristics, where such a deterioration needs to be properly limited; the backlash of the input gear, idler gear, and tail gear had little influence on the load-sharing characteristics of the system.

Author Contributions: Conceptualization, F.G. and R.Z.; methodology, F.G.; software, P.L.; investigation, G.J.; resources, R.Z.; data curation, F.G.; writing—original draft preparation, F.G.; writing—review and editing, R.Z. and G.J.; visualization, F.G.; supervision, P.L. All authors have read and agreed to the published version of the manuscript.

Funding: This research was funded by the National Key R&D Program of China, grant number 2018YFB2001300; National Science and Technology Major Project, grant number J2019-IV-0001-0068; and the National Natural Science Foundation of China, grant numbers 51975273 and 51775265.

Institutional Review Board Statement: Not applicable.

Informed Consent Statement: Not applicable.

Data Availability Statement: Not applicable.

Acknowledgments: This project is supported by the National Key R&D Program of China, grant number 2018YFB2001300, National Science and Technology Major Project, grant number J2019-IV-0001-0068 and the National Natural Science Foundation of China (Grant 51975273 and 51775265).

Conflicts of Interest: The authors declare no conflict of interest.

References

1. Bloomfied, B. Designing Face Gears. *Mach. Des.* **1947**, *19*, 129–134.
2. Buckingham, E. *Analytical Mechanics of Gears*; Dover Publications: New York, NY, USA, 1949; pp. 312–320.
3. Litvin, F.; Zhang, Y.; Wang, J.; Bossier, R.; Chen, Y. Design and Geometry of Face-Gear Drives. *J. Mech. Des.* **1992**, *114*, 642–647. [CrossRef]
4. Heath, G.F.; Bossler, R.B., Jr. *Advanced Rotorcraft Transmission (ART) Program-Final Report*; National Aeronautics and Space Administration: Wahington, DC, USA, 1993; pp. 1–206.
5. Handschuh, R.F.; Lewicki, D.G.; Heath, G.F. Experimental evaluation of face gears for aerospace drive system applications. *NASA Tech. Memo.* **1996**, *107227*, 1–10.
6. Litvin, F.L.; Wang, J.C.; Bossler, R.B.; Bossler, R.B.; Chen, Y.J.D.; Heath, G.; Lewicki, D.G. Application of face-gear drives in helicopter transmissions. *J. Mech. Des.* **1994**, *116*, 672–676. [CrossRef]
7. Handschuh, R.; Lewicki, D.; Bossler, R. Experimental Testing of Prototype Face Gears or Helicopter Transmissions. *Proc. Inst. Mech. Eng.* **1994**, *208*, 129–136. [CrossRef]
8. Filler, R.R.; Heath, G.F.; Slaughter, S.C. Torque splitting by a concentric face gear transmission. In *Proceedings of the 58th American Helicopter Society International Annual Forum, Montreal, QC, Canada, 11–13 June 2002*; American Helicopter Society: Fairfax, VA, USA, 2002.
9. Ding, S.; Liu, S.J.; Hu, Y. Evaluation method of fatigue life for split torque transmission spur gears in helicopter. *J. Cent. South Univ. Sci. Technol.* **2015**, *46*, 135–140. (In Chinese)
10. Zhao, T.Y.; Su, J.P.; Shao, G. Study on Vibration Energy and Fatigue Life of Marine Split Torque Herringbone Gear Transmission System. *J. Eng. Therm. Energy Power* **2021**, *36*, 111–117. (In Chinese)
11. Bodas, A.; Kahraman, A. Influence of Carrier and Gear Manufacturing Errors on the Static Load Sharing Behavior of Planetary Gear Sets. *Jsme Int. J.* **2005**, *47*, 908–915. [CrossRef]
12. Lu, J.H.; Zhu, R.P.; Jin, G.H. Basic-components' offset analysis of planetary gearing in need of loading sharing. *J. Cent. South Univ. Sci. Technol.* **2008**, *39*, 143–148. (In Chinese)
13. Gui, Y.F.; Zhu, R.P.; Fu, B.B. Impact of torsional stiffness on dynamic load sharing coefficient of two-input cylindrical gear split-torque transmission system. *Hangkong Dongli Xuebao/J. Aerosp. Power* **2014**, *29*, 2264–2272. (In Chinese)
14. Sun, W.; Li, X.; Wei, J. A study on load-sharing structure of multi-stage planetary transmission system. *J. Mech. Sci. Technol.* **2015**, *29*, 1501–1511. [CrossRef]
15. Mo, S.; Zhang, Y.D.; Wu, Q. Research on multiple-split load sharing of two-stage star gearing system in consideration of displacement compatibility. *Mech. Mach. Theory* **2015**, *88*, 1–15.
16. Mo, S.; Zhang, Y.; Qiong, W. Load Sharing Behavior of Star Gearing Reducer for Geared Turbofan Engine. *Chin. J. Mech. Eng.* **2017**, *30*, 1–8. [CrossRef]
17. Du, J.; Mao, J.; Liu, K. Load-sharing analysis of two-stage three-branch star gearing based on deformation compatibility. *Adv. Mech. Eng.* **2018**, *10*, 1–13. [CrossRef]
18. Dong, H.; Fang, Z.D.; Hu, Y.H. Study on the Load-Sharing Characteristics of an Aeronautical II-Stage Five-Branching Planets Gear Train Based on the Loaded Tooth Contact Analysis. *Math. Probl. Eng.* **2018**, *2018 Pt 4*, 1–18.
19. Wang, J.; Yang, S.; Liu, Y.; Mo, R. Analysis of Load-Sharing Behavior of the Multistage Planetary Gear Train Used in Wind Generators: Effects of Random Wind Load. *Appl. Sci.* **2019**, *9*, 5501. [CrossRef]
20. Heath, G.F.; Filer, R.R.; Tan, J. Development of Face Gear Technology for Industrial and Aerospace Power Transmission; NASA/CR-2002-2011320. 2002. Available online: https://ntrs.nasa.gov/citations/20020062003 (accessed on 13 March 2022).
21. Chun, H.W.; Filler, R.; Tan, J. Analytical Determination of Load Distribution in a Statically Indeterminate Face Gear Transmission. In Proceedings of the AHS International 62nd Annual Forum, Phoenix, AZ, USA, 9–11 May 2006.
22. Zhao, N.; Wang, R.; Jia, Q. Study on the Load Sharing of Face Gear Split Torque Transmission System. *J. Mech. Transm.* **2013**, *37*, 5–8. (In Chinese)
23. Zhao, N.; Li, W.; Hu, T. Quasistatic Load Sharing Behaviours of Concentric Torque-Split Face Gear Transmission with Flexible Face Gear. *Math. Probl. Eng.* **2018**, *2018*, 1–12. [CrossRef]
24. Zhao, N.; Li, W.; Guo, H.; Zhou, R.C. Study on Load Sharing Behavior of the Concentric Torque-split Face Gear Transmission for Helicopter. *J. Mech. Transm.* **2020**, *44*, 10–17. (In Chinese)
25. Dong, J.; Tang, J.; Hu, Z. A semi-analytical method of time-varying mesh stiffness in concentric face gear split-torque transmission system. *J. Mech. Sci. Technol.* **2020**, *34*, 589–602. [CrossRef]
26. Dong, J.; Tang, J.; Hu, Z. Investigation of assembly, power direction and load sharing in concentric face gear split-torque transmission system. *Meccanica* **2019**, *54*, 485–2506. [CrossRef]

27. Dong, J.; Wang, Q.; Tang, J. Dynamic characteristics and load-sharing performance of concentric face gear split-torque transmission systems with time-varying mesh stiffness, flexible supports and deformable shafts. *Meccanica* **2021**, *56*, 2893–2918. [CrossRef]
28. Li, W.; Zhao, N.; Lin, Y.H.; Qiu, P.Y. Study on Dynamic Load Sharing Characteristics of the Concentric Torque Split Face Gear Transmission. *J. Xi'an Jiaotong Univ.* **2020**, *54*, y1–y7. (In Chinese)
29. Mo, S.; Yue, Z.; Feng, Z. Analytical investigation on load-sharing characteristics for multi-power face gear split flow system. *Proc. Inst. Mech. Eng. Part C J. Mech. Eng. Sci.* **2019**, *234*, 095440621987695. [CrossRef]
30. Mo, S.; Yue, Z.; Feng, Z.; Gao, H. Analytical investigation on load sharing characteristics for face gear split flow system. *J. Huazhong Univ. Sci. Technol.* **2020**, *48*, 23–28. (In Chinese) [CrossRef]
31. Wang, Y.; Zhang, Y.D. Parametric Modeling Methods of Orthogonal Spur Face Gear. *Mach. Des. Manuf.* **2014**, 16–19. [CrossRef]
32. Gonzalez-Perez, I.; Fuentes-Aznar, A. Implementation of a finite element model for stress analysis of gear drives based on multi-point constraints. *Mech. Mach. Theory* **2017**, *117*, 35–47. [CrossRef]
33. Gonzalez-Perez, I.; Fuentes-Aznar, A. Implementation of a Finite Element Model for Gear Stress Analysis Based on Tie-Surface Constraints and Its Validation Through the Hertz's Theory. *ASME J. Mech. Des.* **2018**, *140*, 023301. [CrossRef]